A robust method for fracture orientation and density detection from seismic scattered energy

Xinding Fang, Mike Fehler, Zhenya Zhu, Tianrun Chen, and Daniel Burns, MIT Earth Resources Laboratory*

SUMMARY

The measurements of fracture parameters, such as fracture orientation, fracture density and fracture compliance, in a reservoir is very important for field development and exploration. Traditional seismic methods for fracture characterization include shear wave birefringence (Gaiser and Dok, 2001; Dok et al., 2001; Angerer et al., 2002; Vetri et al., 2003) and amplitude variations with offset and azimuth (AVOA) (Ruger, 1998; Shen et al., 2002; Hall et al., 2003; Liu et al., 2010; Lynn et al., 2010). These methods are based on the equivalent medium theory with the assumption that fracture dimension and spacing are small relative to the seismic wave length, so a fracture zone behaves like an equivalent anisotropic medium. But fractures on the order of seismic wave length are also very important for enhanced oil recovery, and they are one of the important subsurface scattering sources that generate scattered seismic waves.

Willis et al. (2006) developed the Scattering Index method to extract the fracture scattering characteristics by calculating the transfer funtion of a fracture zone. This method has two sources of uncertainty: (1) calculation of the transfer function is sensitive to the analysis time window; (2) the interpretation of the transfer function is based on the assumption that the background reflectivity of the medium is white. Here we propose a modification of the SI methods that addresses these issues and leads to a more robust fracture characterization.

METHODOLOGY

In order to understand the relationship between the transfer function and fracture scattering, a simplified three layer model (Figure 1) is used to study the process of fracture scattering. We assume that fractures are only present in the middle layer and layer interfaces exist both above and below the fractured layer. For simplicity, the data acquisition is assumed to be in one direction first, the azimuth effect will be discussed later. In Figure 1, the wave field reflected from layers above the fracture zone is

$$O_1(\omega) = r_1(\omega) \cdot I(\omega) \tag{1}$$

where $r_1(\omega)$ is the reflectivity of the layers above the fracture zone and $I(\omega)$ is the incident wave field, ω is angular frequency.

When the wave field propagates into the fracture zone, it generates fracture scattered waves, if fractures are vertical or subvertical, which is the general state of fractures present in a reservoir due to overburden stress, most of the scattered waves will propagated downward (Fang et al., 2010), so the downgoing trasmitted waves can be express as

$$T(\omega) = I(\omega) + S(\omega) \tag{2}$$

where $S(\omega)$ denotes the downgoing scattered waves.

Based on the assumption of the stationarity of the incident seismic wavelet, we can represent the downgoing scattered waves

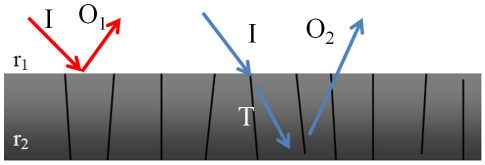

Figure 1: Cartoon showing how incident waves I are reflected by layers above and below the fracture zone. The gray horizontal zone with vertical black lines denotes the fracture zone, O_1 and O_2, respectively, are waves reflected back by layers above and below the fracture zone, of which the reflectivities are r_1 and r_2, respectively. T is the transmitted waves.

as a convolution of the fracture systems transfer function and the incident wave field:

$$S(\omega) = f(\omega) \cdot I(\omega) \tag{3}$$

where $f(\omega)$ is the transfer function for fracture scattering.

By substituting Equation 3 into Equation 2, we get

$$T(\omega) = I(\omega) \cdot [1 + f(\omega] \tag{4}$$

Equation (4) is the Born approximation. The downgoing wave field T is reflected back to the fracture zone by reflectors below it, and the upgoing trasmitted waves generate scattered waves again, thus we can express the upgoing wave field O_2 as

$$O_2(\omega) = r_2(\omega) \cdot T(\omega) \cdot [1 + f(\omega)] = r_2(\omega) \cdot I(\omega) \cdot [1 + f(\omega)]^2 \tag{5}$$

where $r_2(\omega)$ is the reflectivity of the lower reflectors.

In Equation 5, we assume the transfer function $f(\omega)$ is indentical for downgoing and upgoing waves. The physics behind this assumption is that fractures are subvertical and there is no preferential dip direction. Thus, the transfer function of the fracture zone is

$$TF(\omega) = \frac{O_2(\omega)}{O_1(\omega)} = \frac{r_2(\omega)}{r_1(\omega)} \cdot [1 + f(\omega)]^2 \tag{6}$$

We define the fracture transfer function as

$$FTF(\omega) = |1 + f(\omega)| = \left| \frac{TF(\omega)}{TF^0(\omega)} \right|^{1/2} \tag{7}$$

where $TF^0(\omega) = r_2(\omega)/r_1(\omega)$ is the matrix transfer function.

The background matrix response can not be measrued directly in the field, but the scattered waves can be reduced by stacking through an appropriate way, so the stacked data can be used to estimate the background reflectivity. Thus, the matrix transfer function can be expressed as

$$TF^0(\omega) = \frac{O_2^0(\omega)}{O_1^0(\omega)} \tag{8}$$

where $O_1^0(\omega)$ and $O_2^0(\omega)$ are data after stacking.

Therefore, the fracture transfer function can be rewritten as

$$FTF(\omega) = \left| \frac{TF(\omega)}{TF^0(\omega)} \right|^{1/2} = \left| \frac{O_2(\omega) \cdot O_1^0(\omega)}{O_1(\omega) \cdot O_2^0(\omega)} \right|^{1/2} \tag{9}$$

Instead of calculating $f(\omega)$ directly, we prefer to calculate $FTF(\omega)$, because $FTF(\omega)$ can be obtained by simply calculating the amplitude spectrum of the data. So the result is less sensitive to the analysis time window and thus more robust. In the calculation of Equation 9, a water level is added to the denominator to avoid instability, and multi-taper spectral method (Park et al., 1987) is applied to obtain an accurate result.

Willis et al. (2006) pointed out that the fracture scattered wave field acquired normal to the fracture strike direction is incoherent, while the scattered wave field acquired parallel to the fracture strike is much more coherent. After stacking, the scattered waves can be enhanced in the fracture strike direction, while they are eliminated significantly in the direction normal to the fracture strike. Based on these observations, fracture strike can be determined by identifying the acquisition direction with shot records containing coherent scattered waves (Willis et al., 2006). With multi-azimuth data, we stack the data into different azimuthal stacks, as in Willis et al. (2006), and calculate the FTF for each azimuth. So, at each CDP, FTF is a function of frequency and azimuth, thus, Equation 9 can be written as

$$FTF(\omega,\theta)=\frac{\left|O_2(\omega,\theta)\cdot O_1^0(\omega)\right|^{1/2}}{\left|O_1(\omega,\theta)\cdot O_2^0(\omega)\right|^{1/2}} \tag{10}$$

where θ is the stacking azimuth.

Due to interference, the fracture scattered waves are stronger at some frequencies. From both laboratory experiments and numerical simulations, which will be shown later, we find that the fracture scattered waves are stronger at the following frequencies:

$$f_n=n\cdot\frac{V}{2\cdot FS},\quad n=1,2,... \tag{11}$$

where FS is fracture spacing and V is velocity.

A similar relationship between fracture spacing and frequency was observed by Willis et al. (2005), who analyzed the spectral notches of transfer functions extracted from azimuthal stacks, and Grandi et al. (2007), who studied the back scattering of fractures in the F-K domain.

In our study, f_n is defined as the n-th eigen-frequency of the fracture zone, and $f_1=\frac{V}{2\cdot FS}$ is the base eigen-frequency. From both laboratory experiments and numerical simulations, which will be discussed later, we find that, in the direction normal to fracture strike, due to the disruptive nature of fracture scattered waves, notches can be found in FTF at the eigen-frequencies after stacking, in the fracture strike direction, the scattered waves can stack constructively, so peaks appear at the eigen-frequencies after stacking. So the azimuthal variation of $FTF(\omega,\theta)$ is larger at the eigen-frequencies given by Equation 11. The eigen-frequencies and the azimuthal variation of FTF after stacking give information about both fracture orientation and spacing. In order to quantify the azimuthal variation of $FTF(\omega,\theta)$, which can be used to determine the fracture orientation, we define the fracture orientation function as

$$FOF(\theta)=\int_{\omega_1}^{\omega_2}FTF(\omega,\theta)\cdot SDFTF(\omega)\cdot d\omega \tag{12}$$

with

$$SDFTF(\omega)=\sqrt{\frac{1}{N}\sum_{i=1}^{N}\left[FTF(\omega,\theta_i)-\overline{FTF(\omega)}\right]^2} \tag{13}$$

where θ is azimuth, $[\omega_1,\omega_2]$ is frequency window, the weighting function $SDFTF(\omega)$ is the azimuthal standard deviation of FTF, $\overline{FTF(\omega)}$ is the mean of the FTF at frequency ω, N is the number of azimuthal stacks.

Because the azimuthal variation of $FTF(\omega,\theta)$ is larger at the eigen-frequencies, $FOF(\theta)$ can achieve higher resolution by preferentially choosing the data at those frequencies through adding the weighting function $SDFTF(\omega)$. The maximum of $FOF(\theta)$ gives the fracture strike direction. The frequency window $[\omega_1,\omega_2]$ should be chosen as the one that contains the fracutre scattered energy.

We want to emphasize that our analysis is based on two important assumptions: (1)azimuthal variation of the scattered energy is induced by subsurface fracture systems; (2)fracture scatterd waves are preserved and enhanced if stacking is conducted along the fracture strike direction. In the following sections, we use both laboratory and numerical simulation data to explore the FTF and FOF.

LABORATORY EXPERIMENT

We built a parallel fracture network model by cutting parallel notches with 5 mm ($\pm$0.5 mm) spacing and 5 mm depth in a Lucite block, then we put this Lucite block on top of another intact Lucite block to form a two-layer model. These two Lucite blocks were coupled by a very thin water layer with thickness less than 0.5 mm, but the fractures are air-filled.

In this experiment, a P-wave source with 500 kHz central frequency and 600 kHz bandwidth and a vertical component transducer were used to generate and record seismic waves on the top surface of the model. The data were collected at 10 different azimuths. For each azimuth, 7 traces with common midpoint were collected and then stacked into a common midpoint stack after normal moveout.

Figure 2 shows the 10 CMP stacks corresponding to acquisitions at 10 different azimuths. For comparison, the CMP stack of 7 traces from a region without fractures is shown as the blue trace labeled 'Control'. In Figure 2, direct arrivals and surface waves have been muted, the strong signals that arrive at about 0.18 ms are the reflection from the bottom of the lower Lucite block, the signals inside the red window are the waves scattered from the fracture zone.

Because there is no layer interface above the fracture zone in the Lucite model, we compute the FTF, which is shown in Figure 3, by using the Control trace to estimate the reflectivity of the interface between the two Lucite blocks. In our analysis, the analysis time window length is 0.05 ms and time sampling is 0.4×10^{-6} s, so the frequency resolution is 20.2 kHz. A higher frequency resolution can be obtained by increasing the length of the time window, however, the window length is restricted by our Lucite model, because the results will be influenced by the P-to-S converted waves from the interface and the surface waves if a longer window is chosen. Because stacking at different azimuths has different effect on the fracture scattered waves, so the $SDFTF(\omega)$, which is shown as

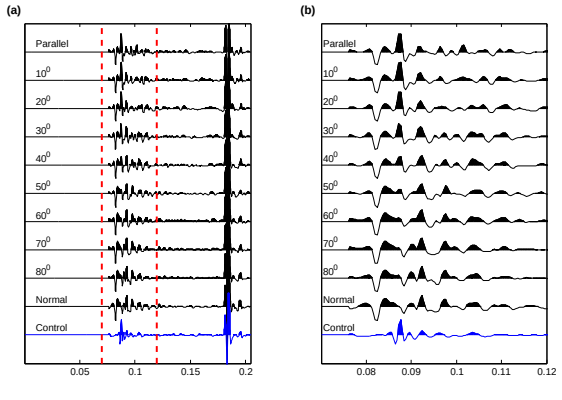

Figure 2: (a) shows CMP stacks at 10 different azimuths, (b) shows the expanded view of the waves in the red window of (a). For each azimuth, 7 traces of offsets 4 cm, 6 cm, 8 cm, 10 cm, 12 cm, 14 cm, and 16 cm were collected and stacked at the common midpoint after applying gain and normal moveout. The acquisition angles are denoted above each trace, 'Parallel'/'Normal' indicates the acquisition is parallel/normal to the fracture strike. 'Control' represents the stack of traces collected at the region without fractures.

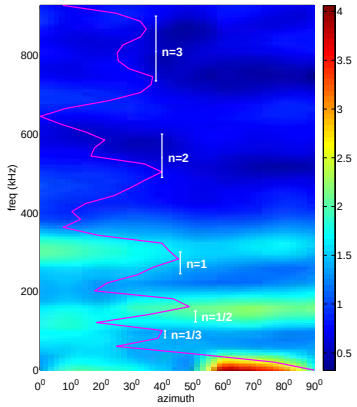

Figure 3: Plot of the FTF of the fracture zone. 0^0 and 90^0 at X-axis represent the direction parallel and normal to the fracture strike, respectively. The magenta curve shows the normalized $SDFTF$ (log scale). The numbers n in the figure are the numbering of the eigen-frequencies predicted by Equation 11. Black error bars show the uncertainties of each eigen-frequency.

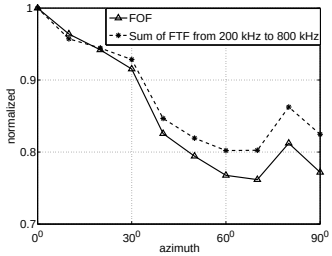

Figure 4: Solid curve shows FOF defined by Equation 12, the frequency window in the calculation is from 200 kHz to 800 kHz. Dash curve is the sum of FTF in the same frequency window without adding the weight.

the magenta curve in Figure 3, has larger value at the eigen-frequencies which can be predicted by Equation 11. From Figure 3, we can clearly see the eigen-frequencies correspond to the numbering of n=1, 2 and 3. n=1/2 and 1/3, respectively, correspond to the interference of every three and four fractures with double and triple fracture spacings. The black error bars show the uncertainties of the predicted eigen-frequencies induced by the error of fracture spacing ($\pm$0.5 mm). For the FTF at the frequency corresponding to n=1/2, the value at 90^0 (normal to fracture strike) is higher than that at 0^0 (parallel to fracture strike), which seems to be conflicting with our statement on the character of azimuthal stacking of fracture scattered waves. To explain this, instead of using the scattering theory, it would be more appropriate to adopt the effective medium theory, since the seismic wave length at this frequency is at least twice of the fracture spacing. From traditional AVOA analysis (e.g. Ruger (1998)), which is based on the effective medium theory, we know that the amplitude of the reflected waves from above a fracture zone is larger if the wave propagation direction is normal to the fracture strike direction, which has higher impedance contrast. The analysis time window chosen for computing the FTF already contains these reflected waves from the fracture zone, which are the waves that arrive at about 0.08 ms in Figure 2. Therefore, in Figure 3, the FTF at high frequency (>200 kHz) agrees with our understanding on fracture scattering, and the FTF at low frequency (<200 kHz) agrees with the effective medium theory. The value of the FTF below 100 kHz may not be reliable, because the source has little energy in this frequency range and spurious high amplitude could be caused by the spectral division.

In Figure 4, the fracture orientation can be clearly determined from the variation of FOF (solid curve), which is defined by Equation 12. Because the central frequency of the source is 500 kHz, so 200kHz-800kHz would be a reasonable frequency window for computing the FOF. The fluctuation of FOF near the normal direction is caused by the low fold in stacking. For comparison, we also show the sum of FTF without adding the weighting function $SDFTF(\omega)$. In Figure 4, we can see that a higher directional resolution can be obtained by adding the weighting function in Equation 12.

NUMERICAL MODELING

A 3D anisotropic, elastic finite-difference code is used in the numerical simulation. In numerical models, fractures are represented by grid cells containing an equivalent anisotropic medium, which is known as the effective medium method (Coates and Schoenberg, 1995). A five layer model with fractures in the third layer is used in our numerical study, Table 1 shows the property of the model. The source wavelet is a Ricker wavelet with a 40 Hz central frequency. Fractures are vertical and parallel to the y axis. Normal and tangential fracture compliance are 10^{-9} m/Pa, which represents gas-filled frac-

Table 1: Parameters of the numerical model

Layer	Thickness (m)	$V_p(m/s)$	$V_s(m/s)$	$\rho(g/cm^3)$
1	200	3000	1765	2.20
2	200	3500	2060	2.25
3	200	4000	2353	2.30
4	200	3500	2060	2.25
5	200	4000	2353	2.30

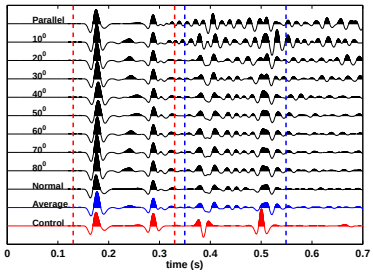

Figure 5: CDP stacks at ten different azimuths. Parallel/Normal represnets that the acquisition direction is parallel/normal to the fracture strike. The traces labeled Average and Control, respectively, correspond to the average of ten CDP stacks and the reference trace, which is obtained from a reference model without fracture. Red and blue windows, respectively, indicate the input and output windows for computing the FTF.

tures. PML (perfectly match layer) is added to all boundaries of the model.

Figure 5 shows the CDP stacks of vertical seismograms in 10 different azimuths. For each azimuth, twenty traces with offsets less than 400 m are chosen and stacked after NMO correction. The blue and red traces in Figure 5, respectively, are the average of CDP stacks of ten azimuths and the control, which is computed from a reference model without fractures. Generally, the background matrix response of a reservoir is unknown, but through numerical study of different models, we find that the average of CDP stacks can be taken as an approximated background response, and this approximation can give us the correct $SDFTF$ and would not alter the major features of the FTF, except for increasing the overall amplitude.

Seven models with fracture spacings of 12 m, 20 m, 32 m, 40 m, 60 m, 80 m and 100 m are simulated in our study, and in order to investigate the robustness of our approach, we also simulate a model which has varying fracture spacing with mean 40 m and standard deviation 4 m. Figure 6a shows the polar plot of the FOFs for all models, which are obatined by applying Equation 12 with calculation frequency window from 10 Hz to 80 Hz. Except for the models with 12m and 20m fracture spacings, the FOFs of all models clearly give the fracture strike direction. This implies that our approach can not resolve the fracture orientation if fracture spacing is much smaller than the seismic wave length, which results in small azimuthal resolution in the FOF.

In Figure 6b, solid curves represent the theoretical eigen-frequencies predicted by Equation 11, and asterisks are the

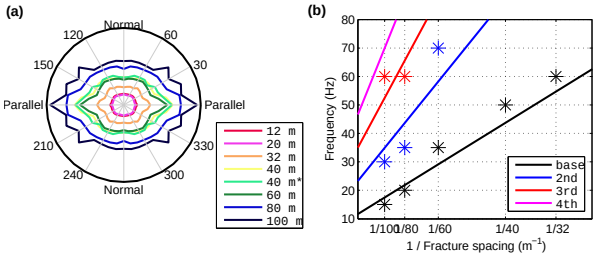

Figure 6: (a) Polar plot of the $SDFTF$s of eight models with different fracture spacings, '40 m*' represents the fracture spacing has a Gaussian distribution with mean 40 m and standard deviation 4 m; (b) Solid curves show the base, 2nd, 3rd and 4th eigen-frequencies predicted by Equation 11. Asterisks are the eigen-frequencies picked from the $SDFTF$s, different color indicates different order of eigen-frequency.

eigen-frequencies obtained from the $SDFTF$s. We can see that the base eigen-frequencies, which are represented by black asterisks, agree well with the therotical values, and the 2nd eigen-frequencies are also consistent with the theoretical values, shown by the blue line. But for higher order eigen-frequencies, as seen from Figure 6b, their theoretical lines become closer to each other, which blurs the distinction of each eigen-frequency and makes it hard to pick the eigen-frequencies accurately. However, this would not affect the accuracy of fracture orientation detection, since the FOF is defined as the sum of FTF over a frequency range, and we only use the base eigen-frequency to estimate the fracture spacing, because the base eigen-frequency is the one that can be picked from data most accurately. Therefore, Figures 6 shows that both fracture orientation and fracture spacing can be extracted from the FTF.

CONCLUSIONS

By applying Equations 11 and 12, the fracture orientation and fracture spacing can be determined from the FTF of the fracture system. Our approach has been tested using both laboratory experiment and numerical modeling. Moreover, the application of this method on the Emilio Field (Italy) provides information about both fracture orientation and fracture spacing, which will be discussed in the presentation. Comparing to the Scattering Index method, the advantage of this approach is its robustness, we find that a stable and accurate result can be obtained from the FTF. However, our approach can only be applied to a fracture network with fracture spacing on the order of seismic wavelength. In fracture spacing measurement, we still need to find a better way to determine the base eigen-frequency and to develop an uncertainty analysis method.

ACKNOWLEDGMENTS

This work was funded by the Eni Multiscale Reservoir Science Project within the Eni-MIT Energy Initiative Founding Member Program. Tianrun Chen was supported by an ERL Founding Member postdoctoral fellowship.

REFERENCES

Angerer, E., S. A. Horne, J. E. Gaiser, R. Walters, S. Bagala, and L. Vetri, 2002, Characterization of dipping fractures using ps mode-converted data: SEG Technical Program Expanded Abstracts, **21**, 1010–1013.

Coates, R., and M. Schoenberg, 1995, Finite-difference modeling of faults and fractures: Geophysics, **60**, 1514.

Dok, R. V., J. Gaiser, and J. Markert, 2001, Green river basin 3-d/3-c case study for fracture characterization: Common-azimuth processing of ps-wave data: SEG Technical Program Expanded Abstracts, **20**, 768–771.

Fang, X., M. Fehler, T. Chen, and D. Burns, 2010, Sensitivity analysis of fracture scattering: SEG Technical Program Expanded Abstracts, **29**, 2340–2345.

Gaiser, J., and R. V. Dok, 2001, Green river basin 3-d/3-c case study for fracture characterization: Analysis of ps-wave birefringence: SEG Technical Program Expanded Abstracts, **20**, 764–767.

Grandi, S., M. Willis, D. Burns, and M. Toksoz, 2007, Analysis of scattered signal to estimate reservoir fracture: Annual Sponsors' Meeting of the Massachusetts Institute of Technology Earth Resources Laboratory.

Hall, S., J. Kendall, et al., 2003, Fracture characterization at Valhall: Application of P-wave amplitude variation with offset and azimuth (AVOA) analysis to a 3D ocean-bottom data set: Geophysics, **68**, 1150.

Liu, E., G. Zelewski, C.-P. Lu, J. Reilly, and Z. J. Shevchek, 2010, Seismic fracture prediction using azimuthal avo analysis in a middle east carbonate field: workflow and mitigation of overburden effects: SEG Technical Program Expanded Abstracts, **29**, 268–272.

Lynn, H., S. R. Narhari, S. Al-Ashwak, V. K. Kidambi, B. Al-Qadeeri, and O. Al-Khaled, 2010, Pp azimuthal-amplitudes and -acoustic impedance for fractured carbonate reservoir characterization: SEG Technical Program Expanded Abstracts, **29**, 258–262.

Park, J., C. Lindberg, and F. Vernon, 1987, Multitaper spectral analysis of high-frequency seismograms: J. geophys. Res, **92**, 675–12.

Ruger, A., 1998, Variation of P-wave reflectivity with offset and azimuth in anisotropic media: Geophysics, **63**, 935.

Shen, F., J. Sierra, D. Burns, and M. Toksoz, 2002, Azimuthal offset-dependent attributes applied to fracture detection in a carbonate reservoir: Geophysics, **67**, 355.

Vetri, L., E. Loinger, J. Gaiser, A. Grandi, and H. Lynn, 2003, 3D/4C Emilio: Azimuth processing and anisotropy analysis in a fractured carbonate reservoir: The Leading Edge, **22**, 675.

Willis, M., D. Burns, R. Rao, B. Minsley, M. Toksoz, and L. Vetri, 2006, Spatial orientation and distribution of reservoir fractures from scattered seismic energy: Geophysics, **71**, O43.

Willis, M., R. Rao, D. Burns, and M. Toksoz, 2005, Fracture spacing and orientation estimation from spectral analysis of azimuth stacks: Annual Sponsors' Meeting of the Massachusetts Institute of Technology Earth Resources Laboratory.